

# A-Graph: A Unified Graph Representation for At-Will Simulation across System Stacks

Daniel Price

Department of ECE

University of Central Florida  
Orlando, USA  
daniel.price@ucf.edu

Prabhu Vellaisamy

Department of ECE

Carnegie Mellon University  
Pittsburgh, USA  
pvellais@andrew.cmu.edu

Patricia Gonzalez

Department of Computer Science

Lawrence Berkeley National Laboratory  
Berkeley, USA  
lg4er@lbl.gov

George Michelogiannakis

Department of Computer Science  
Lawrence Berkeley National Laboratory  
Berkeley, USA  
mihelog@lbl.gov

John P. Shen

Department of ECE  
Carnegie Mellon University  
Pittsburg, USA  
jpshen@cmu.edu

Di Wu

Department of ECE  
University of Central Florida  
Orlando, USA  
di.wu@ucf.edu

**Abstract**—As computer systems continue to diversify across technologies, architectures, applications, and beyond, the relevant design space has become larger and more complex than ever before. Given such trends, design space exploration (DSE) at early stages is critical to ensure agile development towards optimal performance and cost. Industry-grade electronic design automation (EDA) tools directly take in RTL codes and report accurate results, but do not perform DSE. Recent works have attempted to explore the design space via simulation. However, most of these works are domain-specific and constrain the space that users are allowed to explore, offering limited flexibility between technologies, architecture, and applications. Moreover, they often demand high domain expertise to ensure high accuracy. To enable simulation that is agnostic to technology, architecture, and application at any granularity, we introduce Architecture-Graph (*A-Graph*), a graph that unifies the system representation surrounding any arbitrary architecture, application, software, architecture, and circuit. Such a unified representation distinguishes *A-Graph* from prior works focusing on a single stack, and allows users to freely explore the design space across system stacks. To fully unleash the potential of *A-Graph*, we further present *Archx*, a framework that implements *A-Graph* to explore the large design space surrounding target architecture. *Archx* is user-friendly in two ways. First, *A-Graph* has an easy-to-use programming interface to automatically generate and sweep design points under user constraints, boosting the *programmability*. Second, *A-Graph* adopts scope-based metric retrieval to analyze and understand each design point at any user-preferred hierarchy, enhancing the *explainability*. We conduct extensive case studies and demonstrate that *A-Graph* generalizes well across technologies, architecture, and applications with high simulation accuracy. Overall, we argue that *A-Graph* and *Archx* serve as a foundation to simulate both performance and cost at will.

## I. INTRODUCTION

Computer architecture has been considered to enter a new golden age [30], where new technologies, new architecture, new applications are all blooming. Despite the dominant CMOS technology, more exotic circuit technologies are emerging, such as memristors [74], [14], [40], [17], [89], [80], superconducting [5], [18], [63], [28], [47], [27], [75],

TABLE I: Comparing simulators for hardware cost estimation. DSL is for domain specific language. HDL is for hardware description language. acc is for accelerator.

Design	Goal	Flexi- bility	Program- mability	Explain- ability
Charm [20]	Arch perf & cost	Pre-RTL	DSL	No
Aladdin [65]	SoC perf & cost	Pre-RTL	C	No
Accelergy [84]	AI acc cost	Pre-RTL	DSL	No
SNSV2 [85]	SoC Cost	Post-RTL	HDL	No
DSAGEN [79]	Spatial acc chip gen	Post-RTL	C & #pragma	No
OverGen [45]	FPGA chip gen			
TNNGen [77]	Func sim & chip gen	Post-RTL	PyTorch & HDL	No
<i>Archx</i> (ours)	Perf & cost	Pre-RTL	DSL	Yes

photronics [24], [66], [25], [7], [59], [76], quantum [53], [64], [35], [62], [10], [57], and more (even mushroom [39]). These new technologies instigate new architecture organization of computing systems. For example, memristors ignite neuromorphic computing [44], [29], [1], [6]. Both superconducting and photonics are envisioned to instigate new architecture for artificial intelligence (AI) [28], [42], [2] and quantum computing [23], [3], [18]. New applications naturally arise, such as AI for protein structure prediction [36], physics simulation [31], cryogenic sensing [12], [72], etc. While these new technologies, architecture and applications promise substantial gains, evaluating their end-to-end performance and cost is prohibitive, due to the large design space and the slow, or even immature, design flow, across the system stacks of application, software, architecture and circuit. Therefore, fast design space exploration (DSE) via simulation is critical for agile development. For example, for circuit technologies, there are simulators for memristors [87], superconducting circuits [22], photonics [13], and more. For architecture, there also exist simulators to explore computer architecture de-

sign space [20], [9], [60], [65], [61], [8], [86]. Regarding applications, there are more, e.g., Timeloop [55], MEASTRO [38], CoSA [33], ASTRA-sim [81] for AI with a focus on general matrix multiply (GEMM), CAMJ for visual computing [46], UnarySim [82], uSystolic-Sim [83], and Carat [54] for unary computing, SuperNeuro [21] and SATA [90] for neuromorphic computing, Rosé [52] for robotics, etc.

**Problem:** Despite being sufficiently accurate, most existing simulators fall short in one or more among flexibility, programmability, and explainability. We summarize the comparison of existing frameworks for hardware cost evaluation in Table I. First, these simulators are not flexible enough to freely explore the vast design space. They typically examine only a specific system stack, and are increasingly insufficient if users want to optimize multiple stacks simultaneously via co-design. Furthermore, when emerging technologies, architecture, and applications are present, together with different evaluation metrics, these simulators often fail. Second, most of these simulators are not fully programmable and are instead hard-wired for a specific purpose. Significant engineering efforts are needed to either repurpose a simulator for different usage, or add design knobs or stacks. Third, most simulators simply simulate the performance and cost in an end-to-end manner and do not allow user to extract the internal details; therefore, it is difficult to understand the design choices. Such deficiencies raise a key question: *how can a simulation framework capture the cross-stack behaviors of the systems accurately, while remaining flexible, programmable, and explainable?*

**Proposal:** To address the flexibility challenge, we construct Architecture-Graph (*A-Graph*), a graph representation that unifies the abstractions of different system stacks, including application, software, architecture, and circuit. Unlike prior graph representations that solely focus on data [65], control [4], or architecture dependencies [79], *A-Graph* encapsulates all these dependencies across system stacks. Therefore, users can simulate at any granularity, thus accurately, at their own will, unlocking *at-will simulation*. On the contrary, prior works can only be as accurate as what the framework allows, decided by the framework designer. *A-Graph* vertically decomposes and hierarchically flattens the system stacks, so that any changes in technologies, architecture, and applications can be reflected in this graph structure by updating nodes and edges properly. Moreover, unlike prior works that report fixed metrics, *A-Graph* considers metrics flexible rather than fixed and allows users to define their own metrics and units for different technologies, architecture, and applications. One example is that circuit area in CMOS and superconducting technologies is measured in  $mm^2$  and the number of Josephson Junctions (JJ), respectively. This is achieved by defining patterns for graph traversal that can be shared by multiple metrics, and calculating metrics can be done via simple graph traversal.

To unleash the potential of *A-Graph*, we develop *Archx* to implement *A-Graph* at its core to materialize *A-Graph* for arbitrary technology, architecture, and application. Furthermore, we develop an easy-to-use front-end programming interface

to enhance programmability and design scope-based metric retrieval to improve explainability. The programming interface allows users to define the full *A-Graph* at each system stack easily, avoiding manually writing hundreds of raw configuration files, which are error-prone. It also constrains the design space and generates design points within those constraints to sweep through during simulation, avoiding blindly exploring the entire space. Moreover, *Archx* is equipped with scope-based metric retrieval to facilitate rapid analysis of design choices. This retrieval allows to hierarchically analyze the design space at any granularity and understand the design point via rich logs during graph traversal.

The contributions of this work are as follows:

- To explore the large design space across technologies, architecture, and applications, we innovate *A-Graph* to unify the system representations across applications, software, architectures, device technologies, and circuits in one single graph. *A-Graph* unlocks at-will simulation at any granularity and calculates metrics via pattern-based graph traversal.
- To unleash the potential of *A-Graph*, we develop *Archx* that implements *A-Graph* with high programmability and explainability. *Archx* is equipped with an easy-to-use programming interface to automatically generate and sweep design points under user constraints. *Archx* also adopts scope-based metric retrieval to analyze and understand each design point at any user-preferred granularity.
- We validate *A-Graph* and *Archx* with diverse case studies across technologies (i.e., CMOS and superconducting), architecture (i.e., binary and neuromorphic computing), and applications (i.e., signal processing and GEMM) with high accuracy, demonstrating the effectiveness of *A-Graph* and *Archx* towards at-will simulation.

This paper is organized as follows. Section II reviews the background. Then Section III and IV detail our proposed *A-Graph* and *Archx*. Next, Case studies are presented in Section V and VI. Finally, Section VII and VIII discuss and conclude this paper.

## II. BACKGROUND AND MOTIVATION

### A. EDA Workflow

The EDA workflow plays a central role in semiconductor design, facilitating the transformation of high-level specifications into fabrication, while providing accurate post-silicon PPA (power, performance, area) estimates throughout the process flow. EDA flows consist of a sequence of steps, including RTL coding, logic synthesis, physical design (including floorplanning, placement, clock tree synthesis (CTS), and routing), and verification to achieve signoff. Industry-grade EDA tools from Cadence and Synopsys are commonly employed to orchestrate these flows. However, in addition to prohibitively high license costs limiting access, this flow usually demands expert intervention for each stage for high accuracy, as well as lengthy runtime, e.g., spanning from hours to days. All these factors prevent EDA tools from rapid DSE.

## B. Performance and Cost Modeling

Due to the excessive time in EDA tools, many designers rely on simulators for fast performance and cost modeling, which typically trade off accuracy for speed. A comprehensive comparison of prior performance and cost simulators is provided in Table I. These simulators are generally separated into two categories: pre-RTL or post-RTL. Pre-RTL models simulate performance and cost directly from high-level architecture descriptions [65], while post-RTL models either generate RTL from these architecture descriptions [79], [45], [77] or use RTL implementations to refine estimations [85]. These simulators also vary in their expertise requirements, some requiring simple implementations of architecture behavior (e.g., equations [20]), whereas others require deep implementation knowledge (e.g., multi-core C programming [65], [79], [45], RTL implementation [85], [77]).

**Motivation example:** However, most existing simulators operate at only one level of abstraction. In practice, this results in either simplified, equation-based models that capture high-level architecture dependencies, or highly detailed implementations that demand specialized expertise beyond general architecture design (e.g., multi-core C programming or RTL implementation). This narrow focus restricts frameworks to being either flexible but coarse-grained, or fine-grained but burdened by complex hardware specifics. Consequently, their flexibility and accuracy remain inherently constrained by the level of abstraction they target.

## C. Neuromorphic Computing

Recent advancements in AI have caused growing bottlenecks of Von Neumann architecture, thus reinstating interest in brain-inspired, event-driven neuromorphic computing, spiking neural networks (SNNs) [26], [88], [58]. Temporal neural networks (TNNs) [67], [69], [68], [43], [70], [71], a special class of SNNs, utilize spike-timing processing for efficient continuous online clustering. Recent developments in TNN advancements include a microarchitecture model in 45nm CMOS [50], a custom macro suite of highly optimized TNN building blocks [51] augmenting the ASAP7 process design kit (PDK) [77], and automated PyTorch-to-layout translation of single-layer TNNs for time-series applications [15].

**Motivation example.** With diverse SNN implementations (e.g., backpropagation vs. STDP learning, event-based vs. temporal-based encoding and processing), the architecture design space rapidly expands, necessitating efficient simulation and evaluation at varying granularities. The simulation granularity ranges from spike behavioral models at ms scale to cycle-accurate RTL emulations and full analog circuit-level SPICE simulations, where finer granularity captures synaptic dynamics and membrane potentials at ns scale but incur runtime overheads compared to coarser granularity.

## D. Superconducting

Superconductors are metals that exhibit zero electrical resistance at low temperatures, e.g., 10mK~70mK, promising

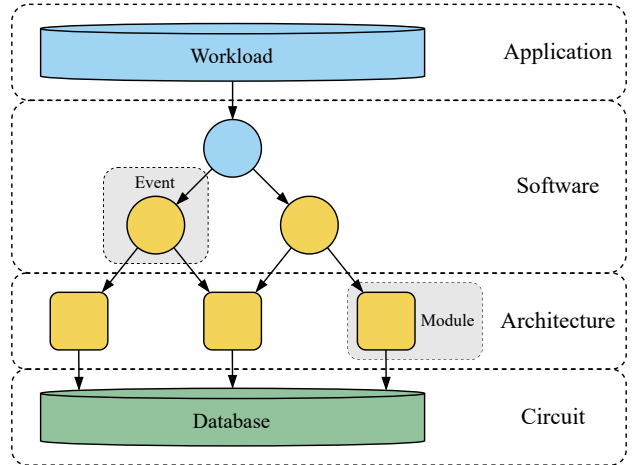


Fig. 1: Overview of *A-Graph*.

ultra-low power and ultra-high efficiency [73]. A popular superconducting logic family is single flux quantum (SFQ) logic, which uses the Josephson Junction (JJ) as its fundamental switching element [73], [41]. Superconducting circuits transmit information by quantizing magnetic flux, encoding data as discrete flux quanta (spikes) rather than continuous voltage levels [73], achieving a substantial decrease in power consumption compared to conventional CMOS designs [48], [32]. Moreover, superconducting logic enables significantly higher clock frequencies than CMOS [16], [41]. Building on this spike-based operation, recent works have introduced unary logic in superconducting systems, namely U-SFQ [28], [27].

**Motivation example:** As superconducting technologies continue to advance, there is a growing need for architecture simulation frameworks for early DSE. Through DSE, designers can identify what applications the technology can have most impact for, or how to restructure the architecture to fit the underlying technology. Furthermore, the framework also needs to adapt to the specific metric needed, such as measuring the area with the number of JJs, instead of  $mm^2$  in CMOS.

**Takeaway:** Overall, there exists a need for a simulation framework that is capable of evaluating both performance and cost at any granularity using any metric, while remaining technology-, architecture-, and application-agnostic. This need strongly motivates *A-Graph*.

## III. *A-Graph* REPRESENTATION

To maximize the flexibility of simulation, we introduce *A-Graph* as a foundation for simulating performance and cost at will. As shown in Figure 1, the core of *A-Graph* is a weighted directed acyclic graph (WDAG) that represent system events using nodes, and directed dependency between events with weighted edges. The acyclic structure ensures a deterministic evaluation order to aggregate metrics. The weighted edge represents a dependency between events, e.g. how many multiplication and addition events are included in one multiply-accumulate (MAC) event. Through these

weighted connections, *A-Graph* shapes its graph structure to the target system.

Unlike prior works that represent a single type of dependency, (e.g., data [65], control [4], and architecture [79]), *A-Graph* encompasses and flattens multiple type of dependencies across system stacks. *A-Graph* vertically decomposes and hierarchically flattens the system stacks into a unified graph of software events and architecture modules, so that any changes in technologies, architecture, and applications can be reflected by updating nodes and edges properly. Furthermore, due to such a unified graph representation, the simulation granularity, i.e., events, can be arbitrarily chosen based on user preference, achieving at-will simulation.

The following subsections detail the graph construction process, the unified modeling of events across system stacks, and the aggregation of evaluation metrics via graph traversal.

### A. Graph Construction

As shown in Figure 1, *A-Graph* resolves into four abstraction layers, namely *application*, *software*, *architecture*, and *circuit*. Each layer represents a distinct system stack and contributing differently to *A-Graph*'s construction, progressively decomposing *A-Graph* from application-level behavior to circuit-level metrics in a flexible and hierarchical way.

1) *Application*: At the top of the stack, the application layer defines the high-level program or algorithm behavior that serves as the input workload to *A-Graph*, i.e., the root node. The possible dependencies in the workload are not expanded yet; generating a system-specific dependency graph is the goal in the software layer. Note that there could exist multiple workloads simultaneously in one graph.

2) *Software*: The software layer defines the event decomposition that maps the application workload onto the hardware architecture modules. Here, users are required to instantiate the nodes for events and edges for dependencies, together forming the backbone of *A-Graph*. An event can be a *workload event*, a *module event*, or a *subevent of a non-module event*. Each event (except the module event) is associated with a performance model that generates the dependency between its subevents, i.e., computing the weights of outgoing edges, informed by both the workload characteristics from the application layer and the architecture description from the architecture layer. This bidirectional dependence allows *A-Graph* to connect application-level behavior with architecture details, unifying the two in a single event-based model. Moreover, these events are decoupled from each other spatially, i.e., users can define events at their preference. For example, one event can be used in multiple parent events, as long as the graph remains acyclic. Though the weighted edges do not reveal temporal dependencies between events, it does not mean the absence of temporal dependencies. Instead, temporal dependencies of events are captured inside the performance models of the parent event, meaning users have full control on temporal dependencies, in addition to spatial dependencies.

3) *Architecture*: The architecture layer provides the structured architecture description to the software layer, supporting

weight generation in conjunction with the application layer. The structured architecture description is based on architecture modules, e.g., gates, compute units, memory, that serve as leaf nodes of the graph. These module definitions are at user's preference to maximize the flexibility at the architecture level. Event decomposition concludes at leaf modules, where aggregated weights from higher layers are mapped onto concrete architecture modules.

4) *Circuit*: At the bottom of the stack, the circuit layer links architecture modules to hardware implementation metrics. Each module refers to a database of precomputed circuit-level results (e.g., area and power of an multiplier from EDA tools) or the output of cost simulators (e.g., CACTI7 [8]), enabling rapid retrieval of accurate metrics without full system simulation.

### B. Unified Modeling

*A-Graph* simultaneously models the full system stacks, integrating their interactions within a single event-based graph. By tying workloads to software events, *A-Graph* mimics the compilation process for *arbitrary applications*, which can be absent in emerging technologies. By connecting software events to architecture modules, *A-Graph* allows software to map to hardware execution for *arbitrary architecture*, resembling the compiler optimization phase. By bridging architecture modules and circuit metrics, *A-Graph* permits optimized implementation choices for *arbitrary technologies*. All these processes, which are usually decoupled in prior works [20], [65], [79], are now unified in *A-Graph* to produce a unified mapping from applications to architecture and simulate the performance and cost of the full system.

### C. Metric Aggregation

Metric evaluation in *A-Graph* proceeds by traversing the graph in topological order, aggregating along weighted edges until reaching leaf nodes. Metric aggregation can be restricted to any subgraph, allowing to choose a flexible scope for analysis. Weighted edges are treated multiplicatively, scaling metrics according to the number of times an event is invoked by its parent event. This process produces system metrics (e.g., area, power, and latency), that reflect the mapping of application workloads onto architecture modules.

Unlike prior works that hardwire their supported metrics [83], [38], [65], [84], *A-Graph* allows to define arbitrary metrics based on the aggregation pattern. *A-Graph* currently supports three types of aggregation, as visualized in Figure 2.

- *Module* aggregation directly aggregates metrics of leaf architecture modules. This aggregation can be applied to metrics that adhere to pure architecture and circuit implementations, such as area and leakage power.
- *Summation* aggregation treats nodes as additive, accumulating metrics across edges and returning a single total value for each metric. This aggregation can be applied to pure spatial aggregation with no temporal dependencies, such as dynamic energy.

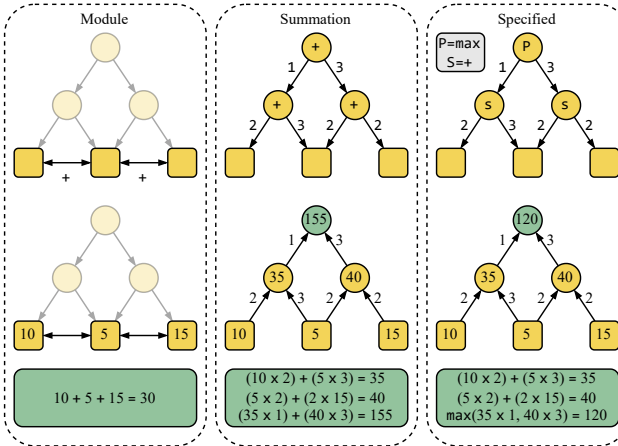


Fig. 2: Patterns of metric aggregation in *A-Graph*. Circles represent events, while squares represent modules. The top row illustrates the functionality of each aggregation type, while the bottom row provides an example, with the final value shown in green. Module aggregation sums module-level metrics. Summation aggregation propagates metrics upward to the root event, multiplying along edges and summing at the end (+). Specified aggregation distinguishes between sequential (S) and parallel (P) events: sequential aggregation behaves like summation, while parallel aggregation multiplies along edges but computes the maximum at each node.

- *Specified* aggregation supports two interaction modes: *sequential* and *parallel*. Sequential events aggregate like summation, accumulating all incoming metrics, while parallel events select only the maximum incoming metric. This aggregation models complex event interactions, such as runtime, where the runtime of two parallel events should be the max of two, rather than the sum.

*A-Graph* highlights the flexibility across arbitrary technology, architecture, application, granularity and metrics, offering a foundation for at-will simulation across system stacks.

#### IV. ARCHX FRAMEWORK

To fully unleash the potential of *A-Graph*, we develop *Archx* that implements *A-Graph* for fast DSE, with high programmability and explainability. *Archx* is user-friendly with two features. First, *Archx* is equipped with an easy-to-use programming interface to automatically generate and sweep design points under user constraints. Second, *Archx* also adopts scope-based metric retrieval to analyze and understand each design point at any user-preferred granularity. The workflow of *Archx* is shown in Figure 3. It starts with generating descriptions to sweep the space, constrained by the user program. Then for each description, the corresponding event graph is generated with all dependencies (i.e., edge weights) updated via simulation. Finally, the event graph will be queried to retrieve the metrics for analysis.

The actual code adopts Python for its simple front-end programming and graph-tool for scalable back-end graph

construction and traversal [56]. We also present a walkthrough example of a MAC array to help understand the usage.

##### A. Front-end Programming Interface

This interface simplifies specifying the configurations for *A-Graph* and allows users to constrain the configurations for sweeping. Listing 1 presents an example of a MAC array (MA) running GEMM operations across multiple configurations. Lines 1–4 instantiate the design and its descriptions, namely the architecture, event, metric, workload, and constraint graph.

1) *Workload Description*: Lines 6–27 define the application-level workloads to be run on the MAC array. We show two workload configurations here, *inner\_product* and *outer\_product*. Each configuration specifies its own parameters by the parameter name and value. *Archx* provides three methods for defining workload parameters:

- Assigned with a single fixed value (line 13).
- Defined as a list with an explicit flag indicating whether it participates in sweeping (line 17).
- Generated dynamically using a sweep object (line 19).

Sweep objects provide a structured mechanism for generating parameter sets, and currently three sweep types are supported:

- *IterationSweep* applies a user-defined function for a specified number of iterations.
- *RangeSweep* applies a function until reaching the end of a defined range.
- *ConditionSweep* continues until a stopping condition is met.

Each sweep object starts from an initial value. In lines 9–10, an *IterationSweep* doubles the batch size across five iterations. More examples of sweep types are discussed in Section IV-A3.

2) *Event Description*: Lines 29–37 define the events within the event graph. Each root event corresponds to a workload. Events propagate from root to leaves by recursively invoking subevents until reaching the architecture modules, which are the leaves and do not have subevents. In Listing 1, the two root events, *inner\_product* and *outer\_product*, each define *MA* as a subevent, which in turn decomposes into the architecture modules (lines 35–36). Each event is associated with a performance model that specifies how it breaks down into subevents, i.e., computes the weights on the edge to each subevent.

3) *Architecture Description*: Lines 39–56 describe the architecture of the MAC array, showing how to define modules.

First, line 46 shows global attributes default to all architecture modules. These global attributes can be overwritten by local attributes in a module. Lines 48–50 showcases that a *cacti7* interface is used as the cost database for *sram*, rather than the global interface *cmos* for compute logic.

Then each module is instantiated with three key properties:

- Property *instance* specifies the number of module instances as a list. In lines 51–52, the multiplier in this  $2 \times 2$  MAC array has an instance of [2, 2].
- Property *tag* groups modules to retrieve metrics during graph traversal. Here, *mult*, *acc*, *ireg*, *wreg*, and *oreg* all belong to one processing element, and share the tag '*pe*'.

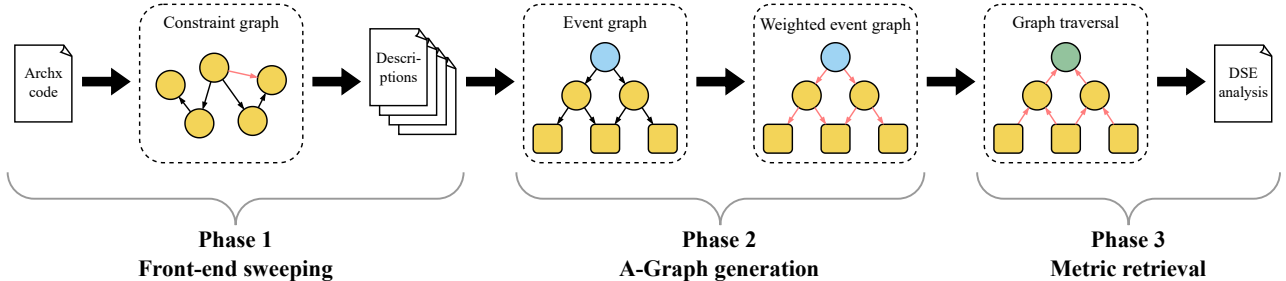


Fig. 3: Overview of Archx.

- Property *query* defines the configuration to retrieve metrics from the module database, and the configuration is database specific. Each query must specify a class to identify the corresponding module metrics. In lines 49-50, *sram* can retrieve its area and power metrics from the *cacti7* interface, with the configuration specified by the *depth*, *width*, and *bank*.

Similar to the workload layer (Section IV-A1), modules can include sweeping objects as parameters. Lines 40-44 show examples of a *RangeSweep*, which doubles both register dimensions until reaching the [4, 4] configuration, and a *ConditionSweep*, which doubles the same dimensions until the first dimension is  $\leq 4$ . Both result in the same sweeping.

4) *Metric Description*: The metric description lists the available metrics and specifies how they are aggregated when traversing the graph generated by Archx. Lines 58-65 list commonly used metrics in CMOS, including *area*, *leakage\_power*, *dynamic\_energy*, *cycle\_count*, and *runtime*. Each metric is given an aggregation type (Section III-C), which define how metrics are retrieved from the graph. Metrics with *specified* aggregation must be defined in the performance model, such as *cycle count* and *runtime*, while metrics with other aggregation types must explicitly exist in the database for querying.

5) *Constraint Graph*: Lines 67-81 define a constraint graph, which restricts sweeping parameters to only viable combinations. Archx introduces three kinds of constraints, namely *injection*, *exclusion*, and *condition*.

- The *injection* constraint introduces one-to-one mapping between parameters, with no combinatorial sweeping happening. It serves as the default constraint type. Lines 68-76 illustrate three examples of injection. Lines 68-70 map all parameters without a condition, i.e., injection is enforced between the instance parameter of all units in a PE. Lines 71-72 apply a condition, but only aligns parameters within a module or workload, *sram* here. Lines 73-76 applies a condition between two objects, either module or workload parameters. When the condition is not met, the parameters remain viable for sweeping.
- The *exclusion* constraint removes combinations where the condition is met. It follows the same structural pattern as injection and can be defined identically, just with the type set to exclusion, as shown in lines 77-81.

- The *condition* constraint combines the behaviors of injection and exclusion, i.e., it applies injection when the condition is met, otherwise it applies exclusion. We omit its example due to the space limit.

After all the descriptions and the constraints are defined, the design is then generated, as shown in line 83.

Figure 4 illustrates how to generate sweeping combinations from these constraints. Right after instantiation, static objects (event and metric descriptions) are directly forwarded generated descriptions in YAML format. Conversely, sweeping objects (architecture and workload descriptions) are used to generate an initial constraint graph. Then all *condition* constraints are split into multiple non-condition constraints, since it is impossible to generate sweepings from condition constraints. Next, we group nodes connected by edges into a subgraph, within which constraints are reduced locally, resulting in a local sweeping. Finally, global sweeping considers all possible combinations between groups. All generated combinations are saved to generate their *A-Graph*.

### B. A-Graph Generation

With *A-Graph* configurations generated, we now simulate all performance models and then generate *A-Graph*.

1) *Performance Model*: Every event in Archx requires a performance model to define the dependencies between its subevent within the event graph. An example of a performance model can be seen in Listing 2, where we define the root event *inner\_product* on lines 1-19 and the subevent *MA* on lines 21-58. All performance models take architecture and workload configurations as input.

The *inner\_product* function defines the number of times an *MA* mapping occurs (its count), which is then placed on the edge from *inner\_product* to *MA*. Lines 6-10 pull relevant parameters from the workload description, represented as a dictionary. In this example, we require the total matrix sizes, the *MA* size, and the batch size to compute the total number of mappings to the *MAC* array, as shown on lines 12-15.

Moreover, the performance model defines both the aggregation type and the factor that metrics will take along an edge. Given that our design includes only a single *MAC* array, each mapping must wait for the previous one to complete, which corresponds to sequential aggregation. If multiple *MAC* arrays were available, mappings could be executed in parallel,

```

1  # Initialize descriptions
2  design = Design(name='mac_array')
3  constraint = design.get_constraint_graph()
4  architecture, event, metric, workload = design.get_descriptions()
5
6  # Add workload configuration and parameters (Application)
7  workload.config(name=['inner_product', 'outer_product'])
8
9  batch_sweep = IterationSweep(value=1, iterations=5,
10                                funct=lambda x:x*2)
11
12  workload.add(config='inner_product', param_name='bitwidth',
13                param_value=16)
14  workload.add(config='inner_product', param_name='dim',
15                param_value=[32, 32, 32], sweep=False)
16  workload.add(config='inner_product', param_name='tile',
17                param_value=[[2, 2], [4, 4], sweep=True])
18  workload.add(config='inner_product', param_name='batch',
19                param_value=batch_sweep)
20  workload.add(config='outer_product', param_name='bitwidth',
21                param_value=16)
22  workload.add(config='outer_product', param_name='dim',
23                param_value=[32, 32, 32], sweep=False)
24  workload.add(config='outer_product', param_name='tile',
25                param_value=[[4, 4], [8, 8], sweep=True])
26  workload.add(config='outer_product', param_name='batch',
27                param_value=batch_sweep)
28
29  # Add events (Software)
30  event.add(name='inner_product', subevent=['MA'],
31             performance_path=performance/product.py)
32  event.add(name='outer_product', subevent=['MA'],
33             performance_path=performance/product.py)
34  event.add(name='MA',
35             subevent=['sram', 'mult', 'acc',
36                       'ireg', 'wreg', 'oreg'],
37             performance_path=performance/mac.py)
38
39  # Add architecture attributes and modules (Architecture)
40  reg_sweep = RangeSweep(value=[2, 2], final=[4, 4],
41                         funct=lambda x: [x[0]*2, x[1]*2])
42  acc_sweep = ConditionSweep(value=[2, 2],
43                             condition=lambda x: x[0] <= 4,
44                             funct=lambda x: [x[0]*2, x[1]*2])
45
46  architecture.attr(technology=45, frequency=400, interface='cmos')
47
48  architecture.add(name='sram', inst=[1], tag=['memory'],
49                  query={'class':'sram', 'depth':[8, 4], 'width':[16, 32],
50                         'bank':1 'interface': 'cacti7'})
51  architecture.add(name='mult', inst=[[2, 2], [4, 4]], tag=['pe'],
52                  query={'class':'multiplier'})
53  architecture.add(name='acc', inst=reg_sweep, tag=['pe'],
54                  query={'class':'accumulator'})
55  architecture.add(name=['ireg', 'wreg', 'oreg'], inst=reg_sweep,
56                  tag=['pe'], query={'class':'register', 'width': 16})
57
58  # Add metrics (Circuit)
59  metric.add(name='area', unit='mm^2', aggregation='module')
60  metric.add(name='leakage_power', unit='mW', aggregation='module')
61  metric.add(name='dynamic_energy', unit='nJ',
62             aggregation='summation')
63  metric.add(name='cycle_count', unit='cycles',
64             aggregation='specified')
65  metric.add(name='runtime', unit='ms', aggregation='specified')
66
67  # Define sweeping constraints
68  constraint.add(inner_product='tile', outer_product='tile',
69                  ireg='inst', wreg='inst', oreg='inst',
70                  mult='inst', acc='inst')
71  constraint.add(sram=['width', 'depth'],
72                  cond=lambda a, b: 256/a == b)
73  constraint.add(a_params={'ireg': 'inst', 'wreg': 'inst',
74                        'oreg': 'inst', 'mult': 'inst', 'acc': 'inst'},
75                  b_params={'sram': 'width'}, type='injection'
76                  cond=lambda a, b: a[0] 8 == b)
77  constraint.add(a_params={'inner_product': 'tile',
78                        'outer_product': 'tile'},
79                  b_params={'inner_product': 'batch',
80                        'outer_product': 'batch'},
81                  type='exclusion', cond=lambda a, b: a*b <= 8)
82
83 design.generate()

```

Listing 1: MAC array front-end code.

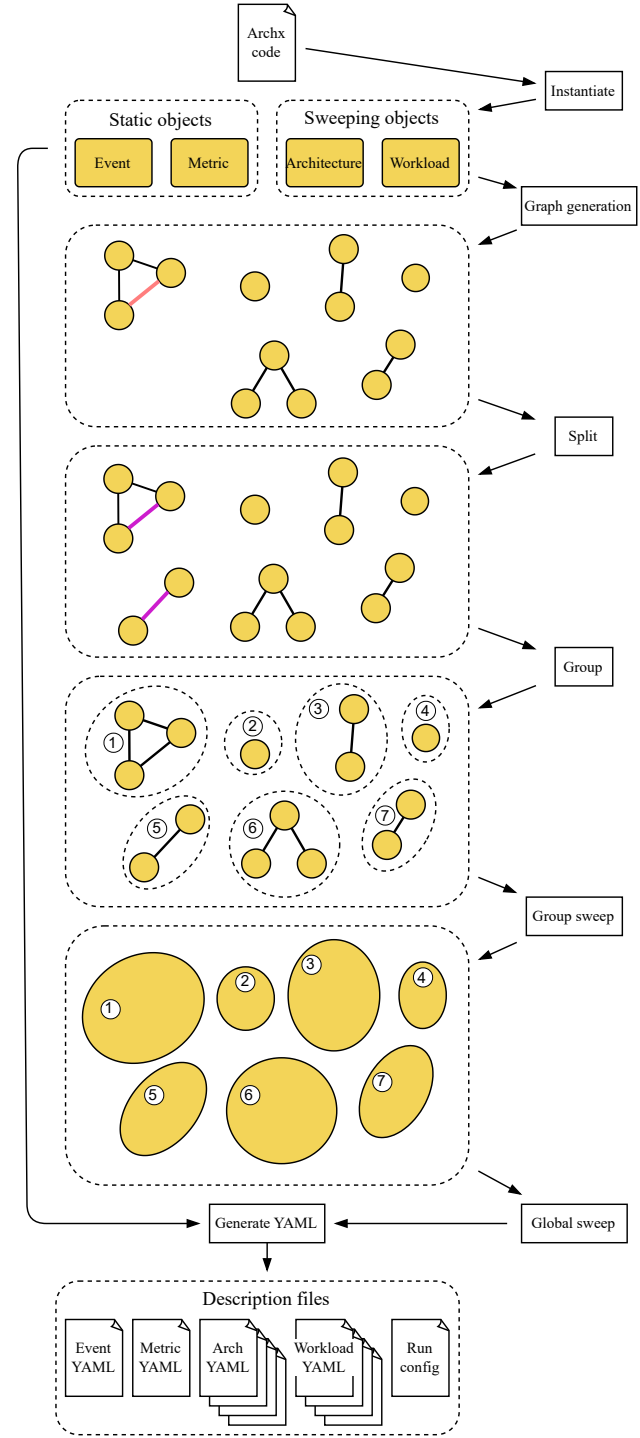


Fig. 4: Archx constraint graph and description generation. Nodes represent workload or module parameters, while edges denote constraints. Red edges indicate condition constraints, and purple edges indicate new non-condition constraints after splitting condition constraints in red.

and the aggregation type could instead be defined as parallel. The factor is a multiplicative scaling factor on the event count along that edge. This factor can serve multiple purposes

depending on the designer's intent, but the most common uses are parameterizing the design or applying hardware utilization. In lines 14–15, applying a factor of 2 to cycle count and

```

1 def inner_product(architecture_dict, workload_dict):
2     perf_dict = {}
3
4     # Retrieve workload parameters
5     config = workload_dict['inner_product']['configuration']
6     m, k, n = config['dim']
7     MA_dim = config['MA']
8     batch = config['batch']
9
10    # Set MA event count
11    mappings = (m/MA_dim) * (k/MA_dim) * (n/MA_dim) * batch
12    ma_dict = {'count': mappings,
13               'aggregation': sequential,
14               'factor': {'cycle_count': 2},
15               'runtime': 2}
16
17    # Add to performance dict
18    perf_dict['subevent'] = {'MA': ma_dict}
19
20    return perf_dict
21
22 def MA(architecture_dict, workload_dict):
23     perf_dict = {}
24
25     # Retrieve workload parameters
26     config = workload_dict['inner_product']['configuration']
27     MA_dim = config['MA']
28
29     # Retrieve architecture parameters
30     mult_events = get_prod(architecture_dict['mult']['instance'])
31     acc_events = get_prod(architecture_dict['acc']['instance'])
32     ireg_events = get_prod(architecture_dict['ireg']['instance'])
33     wreg_events = get_prod(architecture_dict['wreg']['instance'])
34     oreg_events = get_prod(architecture_dict['oreg']['instance'])
35     bitwidth = architecture['ireg']['bitwidth']
36     frequency = architecture['sram']['frequency']
37     sram_bank = architecture_dict['sram']['query']['bank']
38     sram_width = architecture_dict['sram']['query']['width']
39
39     # Calculate cycle count and runtime (specified metrics)
40     perf_dict['cycle_count'] = {'value': 1, 'unit': 'cycle'}
41     perf_dict['runtime'] = {'value': 1/frequency, 'unit': 'ms'}
42
43     # Compute sram event count
44     total_bits = MA_dim * MA_dim * MA_dim * bitwidth
45     sram_events = total_bits / (sram_bank * sram_width)
46
47     mult_dict = {'count': mult_events}
48     acc_dict = {'count': acc_events}
49     ireg_dict = {'count': ireg_events}
50     wreg_dict = {'count': wreg_events}
51     oreg_dict = {'count': oreg_events}
52     sram_dict = {'count': sram_events}
53
54     # Add to performance dict
55     perf_dict['subevent'] = {'mult': mult_dict, 'acc': acc_dict,
56                            'ireg': ireg_dict, 'wreg': wreg_dict,
57                            'oreg': oreg_dict}
58
59     return perf_dict

```

Listing 2: Performance model code.

runtime transforms a single-cycle fused MAC into a 2-cycle non-fused MAC. The MA model defines its subevents in a similar way, which are architecture modules, which do not have performance models.

2) *Building A-Graph*: After all configuration descriptions and performance models are ready, *Archx* builds *A-Graph* for each configuration, as illustrated in Figure 5. ① The event YAML are processed to generate an initial event graph, a WDAG, but with no weights yet. ② The architecture YAML maps a leaf node in the event graph to the corresponding module. ③ The workload YAML loads in the workload configuration as the input for performance simulation. ④ The performance models are loaded to proper event nodes. ⑤ The performance models take the inputs and hierarchically simulate the performance for all events. ⑥ The output of performance models is attached to the corresponding edges, resulting in a fully constructed event graph, *A-Graph*, ready

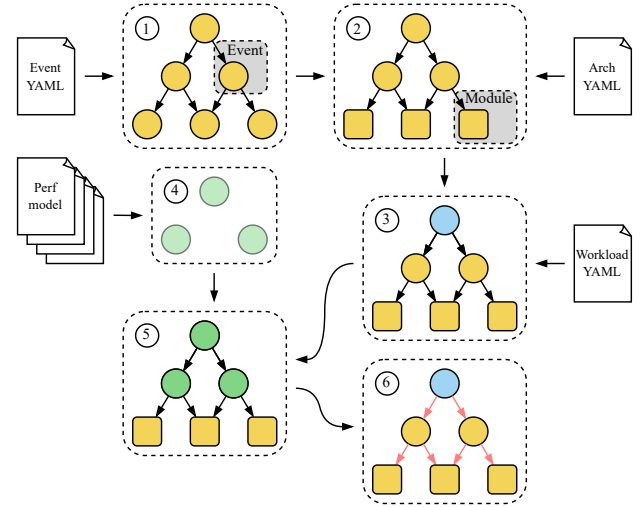


Fig. 5: *A-Graph* generation

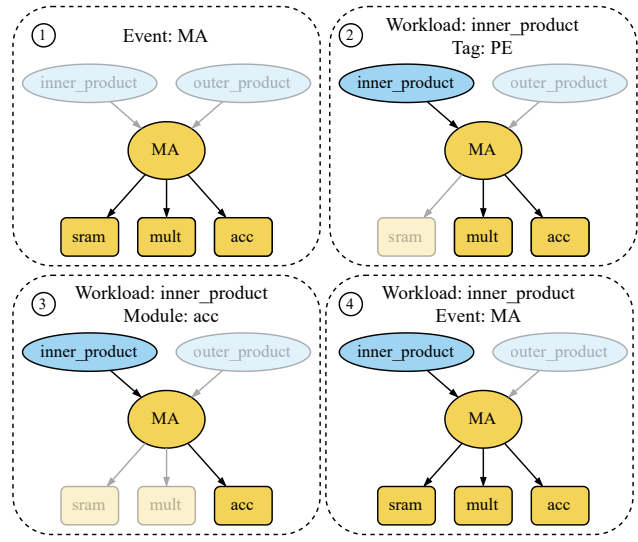


Fig. 6: Scope-based metric retrieval in *Archx*.

for metric retrieval.

### C. Scope-based Metric Retrieval

Retrieving metrics in *Archx* involves selecting a metric (e.g., area, runtime, power), specifying a scope (e.g., workload, event, tag, or module), and graph traversal based on aggregation patterns. Graph traversal always starts from the leaf module nodes upward until reaching the root of the specified scope, allowing focus to be on specific portions of *A-Graph* for hierarchical analysis. Figure 6 showcases different examples of metric retrieval. ① With no workload specified, the metrics of a single MA event will be retrieved. ②-④ all specify *inner\_product* as the scope. ② retrieves the metrics based on tag *pe*, therefore *sram* metrics are excluded, since it is tagged with *pe*, as shown in line 48 in Listing 1. ③ retrieves the metrics of a specific module *acc*, while all others are not counted. ③ concerns the full MA, thus including all modules.

TABLE II: Implemented case studies.

Technology	Node	Application	Architecture
CMOS	45nm	FFT	Butterfly array
		GEMM	Systolic array
7nm		TNN	TNN column
		FIR	Tap array
Superconducting	10 KA/cm <sup>2</sup>	CNN	PE array

## V. EXPERIMENTAL SETUP

To validate the flexibility and accuracy of *A-Graph* and *Archx*, we fully implement five case studies on *Archx*, across different technologies, architecture, and applications. All case study configurations are listed in Table II.

### A. CMOS

We validate the CMOS results of *Archx* against the *full EDA flow* by using Cadence Genus 21.19 for synthesis and Cadence Innovus 19.10 for place-and-route under different process nodes and PDKs (NanGate45 [34], ASAP7 [49], and TNN7 [51]). We set 70% utilization for floorplan for fair comparison. Both fast fourier transform (FFT) and GEMM are processed at 400 MHz clock and 45nm. TNN utilizes a 100 MHz faster clock, and a slower gamma clock of 0.378 MHz clock, as well as ASAP7 and TNN7 PDKs.

### B. Superconducting

We validate superconducting through a finite impulse response (FIR) tag array [27] and a convolutional neural network (CNN) PE array [28]. Both architectures are implemented using the open-source MIT-LL SFQ5ee 10 kA/cm<sup>2</sup> process [37] and simulated with WRSPICE. The reported metrics are area in terms of the number of Josephson Junctions (JJs), dynamic and leakage power, and throughput.

## VI. CASE STUDY

### A. Simulation speedup

Figure 7 shows the runtime comparison between the full EDA flow, module database generation, and *Archx* for CMOS. The runtime of full EDA flow can be  $10^5 \times$  longer than pure *Archx* runtime and  $10^3 \times$  longer than the runtime for *Archx* and database generation, proving *Archx* allows fast DSE.

### B. CMOS

1) *Fast Fourier Transform*: FFT converts a continuous waveform into a discrete time series, thus a signal processing workload [19]. We consider Cooley–Tukey FFT in this study, with each butterfly unit or PE consists of two adders and one multiplier. With inputs  $a_{in}$ ,  $b_{in}$ , and  $w$ , outputs  $a$  and  $b$  are

$$a = a_{in} + b_{in} \cdot w, b = a_{in} - b_{in} \cdot w$$

Here, we implement a flattened FFT, where all butterfly stages are fully pipelined. With  $2N$  inputs, the FFT array has a shape of  $N \times \log_2 N$ . This flattened FFT allows one-time input mapping and does not involve memory access.

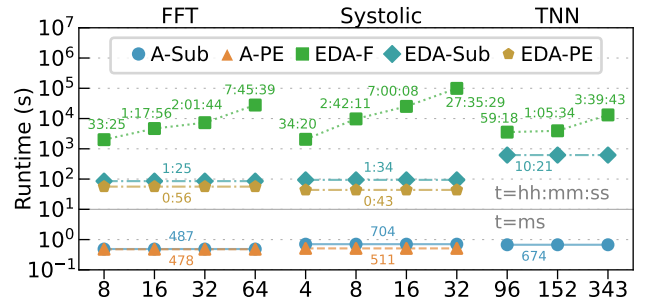


Fig. 7: EDA vs *Archx* (A) runtime for different configurations (x axis). -Sub and -PE denote running *A-Graph* or EDA flow for PE submodules and the full PE. -F denotes running EDA flow for the full design.

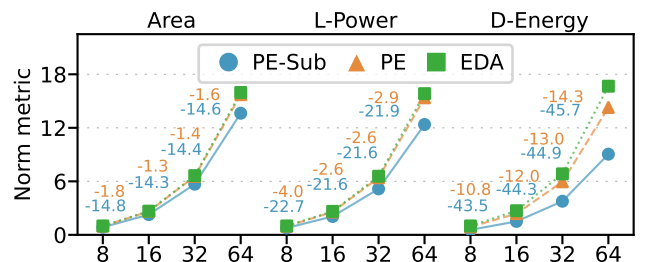


Fig. 8: FFT array-size (x axis) study. All metrics, area, leakage power (L-Power), and dynamic energy (D-Energy), are normalized to the full EDA results of the  $8 \times 3$  array. Relative errors (%) are shown above each plot. PE in orange means *Archx* uses the full butterfly unit directly in the database. PE-Sub means *Archx*'s database uses submodules of a PE.

**Array-size study.** Figure 8 shows the modeling accuracy when scaling the FFT array size. We evaluate array sizes ranging from  $8 \times 3$  to  $64 \times 6$ , with all multipliers and adders in bfloat16 [11]. At the PE granularity, the error is consistently small, capped at 15%. In contrast, the finer PE-Sub granularity shows larger errors when the array size grows. The large error for PE-Sub is the result of submodules not counting the wiring congestion in the full PE, therefore, under-estimating these metrics, mainly the dynamic energy. *These results underscore the importance of selecting the correct module granularity for accurate modeling, despite using arbitrary granularity is feasible.*

**Bitwidth study.** Figure 9 shows 4 different bitwidths using integer multipliers and adders, instead of bfloat16. Adders are configured to ensure no overflow. Here, we only consider the PE level, showing that *Archx* is capable of modeling the FFT array as bitwidth scales with minimal accuracy degradation, achieving error no larger than 9%, and as low as sub 0.1%.

2) *Systolic Array*: We implement weight-stationary systolic arrays with memory in this study for GEMM workloads, the core of AI. Each PE contains a multiplier, an accumulator, registers and extra control logic. Surrounding the PE array

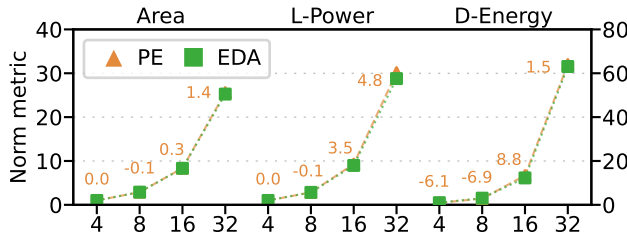


Fig. 9:  $16 \times 4$  FFT bitwidth (x axis) study. All metrics are normalized to the full EDA results of the 4-bit array. Notations follow these in Figure 8.

TABLE III: Systolic array configuration and full *Archx* results. Array dimension is the shape of the systolic array. Matrix dimension represents  $m \times k \times n$  of GEMM.

Array dim.	4x4	8x8	16x16	32x32
Matrix dim.	16x16x16	32x32x32	64x64x64	128x128x128
Throughput (GFLOPs)	6.4	25.6	102.4	409.6
Compute Area ( $\mu\text{m}^2$ )	32.96	127.30	500.09	1982.18
Compute D-Energy (nJ)	16.44	125.00	973.77	7685.43
Compute L-Power (mW)	0.69	2.65	10.38	41.10
Total SRAM (KB)	4	16	64	256
SRAM Area ( $\mu\text{m}^2$ )	22.31	77.25	307.13	1133.88
SRAM D-energy (nJ)	0.60	3.73	26.60	191.91
SRAM L-Power (mW)	0.52	1.82	6.87	24.35

are FIFOs for synchronization, an output accumulator to accumulate partial sums across tiles, and three SRAMs for input, weight, and output.

Table III shows the detailed array configurations, as well as the throughput, and the cost of compute and SRAM. The throughput is perfectly scaled up with 100% array utilization, since the workload size increases proportionally to the array size. The cost of compute does linearly scale with the throughput due to a mixture of scaling to each module. For example, the PE array scales up quadratically with the array width/height, while the accumulator array scales up linearly. The cost of SRAM does not scale linearly, due to similar reasons. However, these results are queried from CACTI7 [8]. If other types of memory exist, users can flexibly switch to a different memory simulator.

**Array-size study.** Figure 10 shows the array scaling of systolic arrays. At smaller array sizes, the PE implementation outperforms the PE-Sub version in modeling accuracy. But at larger array sizes, the PE-Sub implementation outperforms. *Such trade-offs between accuracy and array sizes suggest users to create an ensemble of module databases for different configurations to ensure accuracy.*

**3) Neuromorphic Computing:** Neuromorphic computing is an emerging AI workload that models the behavior of biological neurons. TNNs operate on temporal-coded spikes to reduce switching activity, while SNNs rely on rate-coded spikes. Implemented in ASAP7 and customized TNN7, circuit

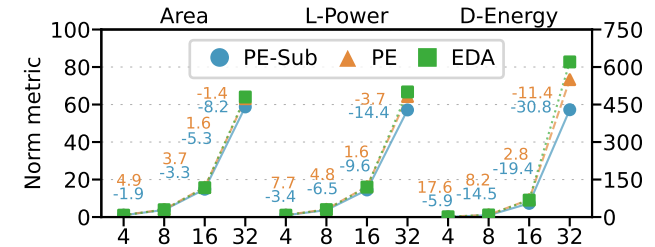


Fig. 10: Systolic array-size (x axis) study. All metrics are normalized to the full EDA results of the  $4 \times 4$  array. Notations follow these in Figure 8.

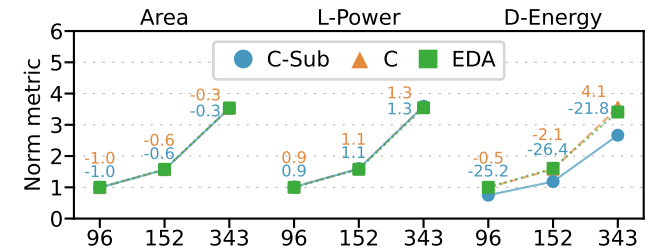


Fig. 11: TNN input-size (x axis) study. Each TNN column (C) has 96, 152, or 343 input neurons, with fixed 2 output neurons. All metrics are normalized to the full EDA results of the 96-input column. C-Sub denotes the fine-grained *Archx* implementation using submodules of the column.

macros are used in this study, in addition to standard cells. We construct a TNN column, a single layer of a TNN, for evaluation.

**Input-size study.** Figure 11 illustrates *Archx*’s modeling of a TNN column architecture across 3 different input neuron sizes. Both area and leakage power show low relative error, capped at 1.3% for both C-Sub and C configurations. The dynamic energy of C-Sub deviates from the full EDA results, due to submodule EDA macro results not capturing the actual circuit fanout load. When capturing this load in the column correctly, the gap is closed, as seen in C.

### C. Superconducting

**1) Finite Impulse Response:** The finite impulse response (FIR) filter returns an impulse response to a finite length input, constructed from sequential taps, each consisting of a shift register, multiplier, and adder. The multiplier and adder can be implemented with a U-SFQ data processing unit (DPU). Leveraging superconducting and unary computing, FIR filters can be implemented with improvements to efficiency at low bit resolutions [27]. We build this superconducting FIR, realizing the capabilities of *Archx* to model signal processing workloads while extending to different technologies.

**Bitwidth study.** Without access to the original throughput and area values, we reproduce their reported trends in Figure 12.

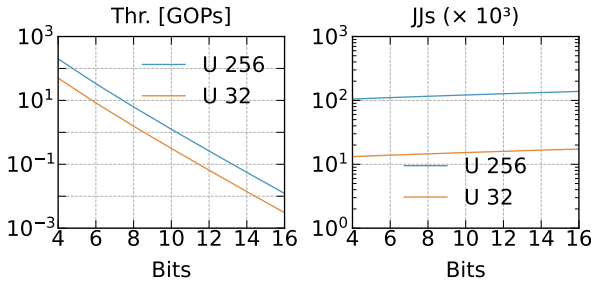


Fig. 12: FIR bitwidth (x axis) study.

TABLE IV: FIR power results.

Metric	Archx	Baseline	Relative error (%)
Dynamic power ( $\mu$ W)	8.125	8.4	-3.27
Leakage power (mW)	8.4	8.4	$1.81 \times 10^{-14}$

TABLE V: Superconducting CNN Results. 3D PE array has a dimension of  $64 \times 64 \times 32$ .

Metric	Archx	Baseline	Relative error (%)
Area (JJ)	13.1M	15.4M	-14.89
Area w/ overhead (JJ)	14.9M	15.4M	-2.97
Power (W)	3.8	3.9	-2.54
Throughput (TMACs)	409.6	409	0.15

Our results yield nearly identical lines for the U-SFQ 32- and 256-tap FIR arrays (U 32, U 256) from [27].

**Power study.** We implement the DPU (U-SFQ multiplier and adder) in *Archx* and model both dynamic and leakage power, as shown in Table IV. Our results exhibit low relative error for both. Given leakage power dominates total power in superconducting designs, the absolute error in total power is also small, yielding nearly identical results to the baseline.

2) *Convolutional Neural Network*: CNNs are deep learning models that excel at feature extraction, specifically for image classification. Similar to GEMMs, these networks require highly parallelized hardware for efficient computation. Prior superconducting work has proposed a 3D PE array, with a scale-up array size of  $64 \times 64 \times 32$  [28]. We implement this 3D PE array in *Archx* to study a matrix convolution workload, reporting area, power, and throughput, as shown in Table V. Our results match the baseline across all metrics other than area. In place of JTL chains, common for long connections, the baseline utilizes passive transmission lines (PTLs) as overhead. Including this overhead reduces the error from 15% to 3%, emphasizing the flexibility. Table VI further breaks down resources that are not reported in [28], demonstrating *Archx*'s capability for metrics retrieval.

TABLE VI: Superconducting array breakdown. S denotes splitters. NDRO is for Non-Destructive Readout memory.

Module	MAC	MAC S	Weight S	Input S	NDRO
Area (JJ)	12.3M	393.2K	393.2K	393.2K	448
Power (mW)	3801.08	785.86	785.86	785.86	0.6

## VII. DISCUSSION

### A. Related Work

1) *Architecture Modeling*: Charm provides a high-level architecture language that expresses relationships between dependent architectural parameters using analytical rather than cycle-level simulation [20]. It builds an internal dependency graph to solve these relationships and apply compiler constraints and optimizations for efficient modeling. Charm supports DSE by letting users explicitly or implicitly specify iterables that sweep automatically. *A-Graph*'s constraint graph limits DSE to practical design points, whereas Charm's constraint system manages relational dependencies. Both use high-level analytical models, but *A-Graph* goes further by decomposing these models into real hardware metrics through cross-stack evaluation.

2) *Performance and Cost Modeling*: There exists prior works that attempt to project architecture predictions by mapping expert C code to pre-synthesized RTL blocks and memory models [65]. Additional works instead leverage look tables to retrieve energy costs from primitive and compound compute and memory components [84]. Finally, recent works extend graph neural networks (GNN) to HDL compilation, generating a hierarchical graph representation for accurate cost estimation [85]. While all are effective, each restricts itself to a specific domain, limiting generality to broader technology, applications, and architecture.

3) *Agile Chip Generation*: Prior efforts have considered chip generation from #pragma annotated C code, mapping execution onto precomputed hardware primitives for both ASIC and FPGA decoupled spatial accelerators [79], [45]. Furthermore, recent work has extended generation to neuromorphic computing, targeting TNN models and architecture [78]. Similarly, these frameworks limit themselves to specific accelerators or architecture, thus not generalizable to emerging technologies, architecture, and application.

### B. Limitations of This Work

Despite everything previously mentioned, one limitation remains in *A-Graph*. *A-Graph* flattens the computational graph across the spatial dimension into event nodes, modeling the performance within each event node, where the temporal relationship of its subevents is preserved. This leaves *Archx* to rely on user expertise to maintain proper spatial and temporal relationships. Given architecture designs for new technologies are usually small in scale, this requirement does not prohibit development. Moreover, maturing compilation tools allow integration of intermediate results into *Archx*. Though raising the

barrier-to-entry, our support for at-will simulation permits simulation at users maximum potential. Like Alladin [65] expects proficient C programming, achieving optimal hardware results requires high expertise when optimizing graph inputs. That said, in emerging technologies, architecture, and applications, it is indeed expected that users own sufficient domain expertise to take advantage of *A-Graph* and *Archx*.

### VIII. CONCLUSION

In the golden age of computer architecture, new technologies, architectures, and applications are rapidly expanding the design space, creating a need for fast exploration. We propose *A-Graph* to unify representations across application, software, architecture, and circuit levels, enabling design space exploration via graph traversal. This unification allows *A-Graph* to support at-will simulation, i.e., simulating at user-defined granularity. Building on these concepts, *Archx* enhances usability with a programming language and scope-based metric retrieval, improving programmability and explainability for novel system design in emerging domains. Extensive case studies demonstrate *A-Graph*’s at-will simulation capabilities, as well as *Archx*’s programmability and explainability.

### REFERENCES

- [1] G. C. Adam, B. D. Hoskins, M. Prezioso, F. Merrikh-Bayat, B. Chakrabarti, and D. B. Strukov, “3-d memristor crossbars for analog and neuromorphic computing applications,” *IEEE Transactions on Electron Devices*, vol. 64, no. 1, pp. 312–318, 2016.
- [2] S. R. Ahmed, R. Baghdadi, M. Bernadskiy, N. Bowman, R. Braid, J. Carr, C. Chen, P. Ciccarella, M. Cole, J. Cooke *et al.*, “Universal photonic artificial intelligence acceleration,” *Nature*, vol. 640, no. 8058, pp. 368–374, 2025.
- [3] K. Alexander, A. Bahgat, A. Benyamin, D. Black, D. Bonneau, S. Burgos, B. Burridge, G. Campbell, G. Catalano, A. Ceballos *et al.*, “A manufacturable platform for photonic quantum computing,” *Nature*, vol. 641, no. 8064, pp. 876–883, 2025.
- [4] F. E. Allen, “Control flow analysis,” *ACM Sigplan Notices*, vol. 5, no. 7, pp. 1–19, 1970.
- [5] P. B. Allen and B. Mitrović, “Theory of superconducting tc,” *Solid state physics*, vol. 37, pp. 1–92, 1983.
- [6] A. Ankit, A. Sengupta, P. Panda, and K. Roy, “Respac: A reconfigurable and energy-efficient architecture with memristive crossbars for deep spiking neural networks,” in *Proceedings of the 54th Annual Design Automation Conference 2017*, 2017, pp. 1–6.
- [7] P. Antonik, N. Marsal, D. Brunner, and D. Rontani, “Human action recognition with a large-scale brain-inspired photonic computer,” *Nature Machine Intelligence*, vol. 1, no. 11, pp. 530–537, 2019.
- [8] R. Balasubramonian, A. B. Kahng, N. Muralimanohar, A. Shafiee, and V. Srinivas, “CACTI 7: New Tools for Interconnect Exploration in Innovative Off-Chip Memories,” *Transactions on Architecture and Code Optimization*, 2017.
- [9] N. Binkert, B. Beckmann, G. Black, S. K. Reinhardt, A. Saidi, A. Basu, J. Hestness, D. R. Hower, T. Krishna, S. Sardashti *et al.*, “The gem5 simulator,” *ACM SIGARCH computer architecture news*, vol. 39, no. 2, pp. 1–7, 2011.
- [10] R. Blatt and C. F. Roos, “Quantum simulations with trapped ions,” *Nature Physics*, vol. 8, no. 4, pp. 277–284, 2012.
- [11] N. Burgess, J. Milanovic, N. Stephens, K. Monachopoulos, and D. Mansell, “Bfloat16 processing for neural networks,” *IEEE Xplore*, 2019.
- [12] L. Cardani, F. Bellini, N. Casali, M. Castellano, I. Colantoni, A. Coppolechia, C. Cosmelli, A. Cruciani, A. D’Addabbo, S. Di Domizio *et al.*, “New application of superconductors: High sensitivity cryogenic light detectors,” *Nuclear Instruments and Methods in Physics Research Section A: Accelerators, Spectrometers, Detectors and Associated Equipment*, vol. 845, pp. 338–341, 2017.
- [13] J. Chan, G. Hendry, A. Biberman, K. Bergman, and L. P. Carloni, “Phoenixsim: A simulator for physical-layer analysis of chip-scale photonic interconnection networks,” in *2010 Design, Automation & Test in Europe Conference & Exhibition (DATE 2010)*. IEEE, 2010, pp. 691–696.
- [14] A. Chanthbouala, V. Garcia, R. O. Cherifi, K. Bouzehouane, S. Fusil, X. Moya, S. Xavier, H. Yamada, C. Deranlot, N. D. Mathur *et al.*, “A ferroelectric memristor,” *Nature materials*, vol. 11, no. 10, pp. 860–864, 2012.
- [15] S. Chaudhari, H. Nair, J. M. Moura, and J. P. Shen, “Unsupervised clustering of time series signals using neuromorphic energy-efficient temporal neural networks,” in *ICASSP 2021-2021 IEEE International Conference on Acoustics, Speech and Signal Processing (ICASSP)*. IEEE, 2021, pp. 7873–7877.
- [16] W. Chen, A. Ryllyakov, V. Patel, J. Lukens, and K. Likharev, “Rapid single flux quantum t-flip flop operating up to 770 ghz,” *IEEE Transactions on Applied Superconductivity*, vol. 9, no. 2, pp. 3212–3215, 1999.
- [17] L. Chua, “Memristor-the missing circuit element,” *IEEE Transactions on circuit theory*, vol. 18, no. 5, pp. 507–519, 2003.
- [18] J. Clarke and F. K. Wilhelm, “Superconducting quantum bits,” *Nature*, vol. 453, no. 7198, pp. 1031–1042, 2008.
- [19] W. Cochran, J. Cooley, D. Favin, H. Helms, R. Kaenel, W. Lang, G. Maling, D. Nelson, C. Rader, and P. Welch, “What is the fast fourier transform?” *Proceedings of the IEEE*, vol. 55, no. 10, pp. 1664–1674, 1967.
- [20] W. Cui, Y. Ding, D. Dangwal, A. Holmes, J. McMahan, A. Javadi-Abhari, G. Tzimpragos, F. Chong, and T. Sherwood, “Charm: A language for closed-form high-level architecture modeling,” in *2018 ACM/IEEE 45th Annual International Symposium on Computer Architecture (ISCA)*, 2018, pp. 152–165.
- [21] P. Date, C. Gunaratne, S. R. Kulkarni, R. Patton, M. Coletti, and T. Potok, “Superneuro: A fast and scalable simulator for neuromorphic computing,” in *Proceedings of the 2023 International Conference on Neuromorphic Systems*, ser. ICONS ’23. New York, NY, USA: Association for Computing Machinery, 2023. [Online]. Available: <https://doi.org/10.1145/3589737.3606000>
- [22] J. A. Delport, K. Jackman, P. Le Roux, and C. J. Fourie, “Josim—superconductor spice simulator,” *IEEE Transactions on Applied Superconductivity*, vol. 29, no. 5, pp. 1–5, 2019.
- [23] X. Ding, Y.-P. Guo, M.-C. Xu, R.-Z. Liu, G.-Y. Zou, J.-Y. Zhao, Z.-X. Ge, Q.-H. Zhang, H.-L. Liu, L.-J. Wang *et al.*, “High-efficiency single-photon source above the loss-tolerant threshold for efficient linear optical quantum computing,” *Nature Photonics*, pp. 1–5, 2025.
- [24] B. Dong, F. Brückerhoff-Plückelmann, L. Meyer, J. Dijkstra, I. Bente, D. Wendland, A. Varri, S. Aggarwal, N. Farmakidis, M. Wang *et al.*, “Partial coherence enhances parallelized photonic computing,” *Nature*, vol. 632, no. 8023, pp. 55–62, 2024.
- [25] B. L. Drake, R. P. Bocker, M. E. Lasher, R. H. Patterson, and W. J. Miceli, “Photonic computing using the modified signed-digit number representation,” *Optical Engineering*, vol. 25, no. 1, pp. 38–43, 1986.
- [26] S. Ghosh-Dastidar and H. Adeli, “Spiking neural networks,” *International journal of neural systems*, vol. 19, no. 04, pp. 295–308, 2009.
- [27] P. Gonzalez-Guerrero, M. G. Bautista, D. Lyles, and G. Michelogiannakis, “Temporal and sqf pulse-streams encoding for area-efficient superconducting accelerators,” in *Proceedings of the 27th ACM International Conference on Architectural Support for Programming Languages and Operating Systems*, ser. ASPLOS ’22. New York, NY, USA: Association for Computing Machinery, 2022, p. 963–976. [Online]. Available: <https://doi.org/10.1145/3503222.3507765>
- [28] P. Gonzalez-Guerrero, K. Huch, N. Patra, T. Popovici, and G. Michelogiannakis, “Toward practical superconducting accelerators for machine learning using u-sfq,” *J. Emerg. Technol. Comput. Syst.*, vol. 20, no. 2, Jun. 2024. [Online]. Available: <https://doi.org/10.1145/3653073>
- [29] Z. He, J. Lin, R. Ewetz, J.-S. Yuan, and D. Fan, “Noise injection adaption: End-to-end reram crossbar non-ideal effect adaption for neural network mapping,” in *Proceedings of the 56th Annual Design Automation Conference 2019*, ser. DAC ’19. New York, NY, USA: Association for Computing Machinery, 2019. [Online]. Available: <https://doi.org/10.1145/3316781.3317870>
- [30] J. L. Hennessy and D. A. Patterson, “A new golden age for computer architecture,” *Commun. ACM*, vol. 62, no. 2, p. 48–60, Jan. 2019. [Online]. Available: <https://doi.org/10.1145/3282307>
- [31] O. Hennigh, S. Narasimhan, M. A. Nabian, A. Subramaniam, K. Tangsali, Z. Fang, M. Rietmann, W. Byeon, and S. Choudhry, “Nvidia

simnet™: An ai-accelerated multi-physics simulation framework,” in *International conference on computational science*. Springer, 2021, pp. 447–461.

[32] Q. P. Herr, A. Y. Herr, O. T. Oberg, and A. G. Ioannidis, “Ultra-low-power superconductor logic,” *Journal of Applied Physics*, vol. 109, no. 10, May 2011. [Online]. Available: <http://dx.doi.org/10.1063/1.3585849>

[33] Q. Huang, M. Kang, G. Dinh, T. Norell, A. Kalaiah, J. Demmel, J. Wawrzynek, and Y. S. Shao, “Cosa: scheduling by unconstrained optimization for spatial accelerators,” in *Proceedings of the 48th Annual International Symposium on Computer Architecture*, ser. ISCA ’21. IEEE Press, 2021, p. 554–566. [Online]. Available: <https://doi.org/10.1109/ISCA52012.2021.00050>

[34] N. Inc., “Nangate Open Cell Library: 45nm open cell standard cell library,” 2009, available at <https://www.nangate.com>.

[35] L. Isenhower, E. Urban, X. Zhang, A. Gill, T. Henage, T. A. Johnson, T. Walker, and M. Saffman, “Demonstration of a neutral atom controlled-not quantum gate,” *Physical review letters*, vol. 104, no. 1, p. 010503, 2010.

[36] J. Jumper, R. Evans, A. Pritzel, T. Green, M. Figurnov, O. Ronneberger, K. Tunyasuvunakool, R. Bates, A. Žídek, A. Potapenko *et al.*, “Highly accurate protein structure prediction with alphafold,” *nature*, vol. 596, no. 7873, pp. 583–589, 2021.

[37] A. F. Kirichenko, S. Sarwana, and D. Gupta, “Advanced SFQ5ee process at MIT Lincoln Laboratory,” in *Proceedings of the IEEE International Superconductive Electronics Conference (ISEC)*, 2003, pp. K4–1.

[38] H. Kwon, P. Chatarasi, M. Pellauer, A. Parashar, V. Sarkar, and T. Krishna, “Understanding reuse, performance, and hardware cost of DNN dataflow: A data-centric approach,” in *Proceedings of the 52nd Annual IEEE/ACM International Symposium on Microarchitecture, MICRO*. ACM, 2019, pp. 754–768.

[39] J. LaRocco, Q. Tahmina, R. Petreaca, J. Simonis, and J. Hill, “Sustainable memristors from shiitake mycelium for high-frequency bioelectronics,” *PLoS One*, vol. 20, no. 10, p. e0328965, 2025.

[40] C. Li, M. Hu, Y. Li, H. Jiang, N. Ge, E. Montgomery, J. Zhang, W. Song, N. Dávila, C. E. Graves *et al.*, “Analogue signal and image processing with large memristor crossbars,” *Nature electronics*, vol. 1, no. 1, pp. 52–59, 2018.

[41] K. Likharev and V. Semenov, “Rsfq logic/memory family: a new josephson-junction technology for sub-terahertz-clock-frequency digital systems,” *IEEE Transactions on Applied Superconductivity*, vol. 1, no. 1, pp. 3–28, 1991.

[42] X. Lin, Y. Rivenson, N. T. Yardimci, M. Veli, Y. Luo, M. Jarrahi, and A. Ozcan, “All-optical machine learning using diffractive deep neural networks,” *Science*, vol. 361, no. 6406, pp. 1004–1008, 2018.

[43] D. Lister, P. Vellaisamy, J. P. Shen, and D. Wu, “Catwalk: Unary top-k for efficient ramp-no-leak neuron design for temporal neural networks,” in *2025 IEEE Computer Society Annual Symposium on VLSI (ISVLSI)*, vol. 1, 2025, pp. 1–6.

[44] C. Liu, B. Yan, C. Yang, L. Song, Z. Li, B. Liu, Y. Chen, H. Li, Q. Wu, and H. Jiang, “A spiking neuromorphic design with resistive crossbar,” in *Proceedings of the 52nd Annual Design Automation Conference*, 2015, pp. 1–6.

[45] S. Liu, J. Weng, D. Kupsh, A. Sohrabizadeh, Z. Wang, L. Guo, J. Liu, M. Zhulin, R. Mani, L. Zhang, J. Cong, and T. Nowatzki, “Overgen: Improving fpga usability through domain-specific overlay generation,” in *2022 55th IEEE/ACM International Symposium on Microarchitecture (MICRO)*, 2022, pp. 35–56.

[46] T. Ma, Y. Feng, X. Zhang, and Y. Zhu, “Camj: Enabling system-level energy modeling and architectural exploration for in-sensor visual computing,” in *Proceedings of the 50th Annual International Symposium on Computer Architecture*, 2023, pp. 1–14.

[47] G. Michelogiannakis, A. Butko, P. Gonzalez-Guerrero, D. Vasudevan, M. Gay Bautista-Jurney, C. Grace, P. Zarkos, and J. Shalf, “Unconventional compute methods and future challenges for superconducting digital computing,” *Frontiers in Materials*, vol. 12, p. 1618615, 2025.

[48] O. A. Mukhanov, “Energy-efficient single flux quantum technology,” *IEEE Transactions on Applied Superconductivity*, vol. 21, no. 3, pp. 760–769, 2011.

[49] S. Naffziger, S.-C. Yang, D. J. Carlberg, B. Sarkar, S. K. Sinha, G. Yeric, and M. Haycock, “ASAP7: A 7-nm finfet predictive process design kit,” in *Proceedings of the 54th Annual Design Automation Conference (DAC)*. ACM, 2017, pp. 1–6.

[50] H. Nair, J. P. Shen, and J. E. Smith, “Direct cmos implementation of neuromorphic temporal neural networks for sensory processing,” *arXiv preprint arXiv:2009.00457*, 2020.

[51] H. Nair, P. Vellaisamy, S. Bhasuthkar, and J. P. Shen, “Tnn7: A custom macro suite for implementing highly optimized designs of neuromorphic tnn,” in *2022 IEEE Computer Society Annual Symposium on VLSI (ISVLSI)*. IEEE, 2022, pp. 152–157.

[52] D. Nikiforov, S. C. Dong, C. L. Zhang, S. Kim, B. Nikolic, and Y. S. Shao, “Rosé: A hardware-software co-simulation infrastructure enabling pre-silicon full-stack robotics soc evaluation,” in *Proceedings of the 50th Annual International Symposium on Computer Architecture*, 2023, pp. 1–15.

[53] J. L. O’brien, “Optical quantum computing,” *Science*, vol. 318, no. 5856, pp. 1567–1570, 2007.

[54] Z. Pan, J. San Miguel, and D. Wu, “Carat: Unlocking Value-Level Parallelism for Multiplier-Free GEMMs,” in *International Conference on Architectural Support for Programming Languages and Operating Systems*, 2024.

[55] A. Parashar, P. Raina, Y. S. Shao, Y.-H. Chen, V. A. Ying, A. Mukkara, R. Venkatesan, B. Khailany, S. W. Keckler, and J. Emer, “Timeloop: A systematic approach to dnn accelerator evaluation,” in *2019 IEEE International Symposium on Performance Analysis of Systems and Software (ISPASS)*, 2019, pp. 304–315.

[56] T. P. Peixoto, “The graph-tool python library,” *figshare*, 2014. [Online]. Available: [http://figshare.com/articles/graph\\_tool/1164194](http://figshare.com/articles/graph_tool/1164194)

[57] J. M. Pino, J. M. Dreiling, C. Figgatt, J. P. Gaebler, S. A. Moses, M. Allman, C. Baldwin, M. Foss-Feig, D. Hayes, K. Mayer *et al.*, “Demonstration of the trapped-ion quantum ccd computer architecture,” *Nature*, vol. 592, no. 7853, pp. 209–213, 2021.

[58] N. Rathi, I. Chakraborty, A. Kosta, A. Sengupta, A. Ankit, P. Panda, and K. Roy, “Exploring neuromorphic computing based on spiking neural networks: Algorithms to hardware,” *ACM Computing Surveys*, vol. 55, no. 12, pp. 1–49, 2023.

[59] C. Ríos, N. Youngblood, Z. Cheng, M. Le Gallo, W. H. Pernice, C. D. Wright, A. Sebastian, and H. Bhaskaran, “In-memory computing on a photonic platform,” *Science advances*, vol. 5, no. 2, p. eaau5759, 2019.

[60] A. F. Rodrigues, K. S. Hemmert, B. W. Barrett, C. Kersey, R. Oldfield, M. Weston, R. Risen, J. Cook, P. Rosenfeld, E. Cooper-Balis *et al.*, “The structural simulation toolkit,” *ACM SIGMETRICS Performance Evaluation Review*, vol. 38, no. 4, pp. 37–42, 2011.

[61] P. Rosenfeld, E. Cooper-Balis, and B. Jacob, “Dramsim2: A cycle accurate memory system simulator,” *IEEE computer architecture letters*, vol. 10, no. 1, pp. 16–19, 2011.

[62] T. Rudolph, “Why i am optimistic about the silicon-photonic route to quantum computing,” *APL photronics*, vol. 2, no. 3, 2017.

[63] E. Savitskii, *Superconducting materials*. Springer Science & Business Media, 2012.

[64] D. Schrader, I. Dotsenko, M. Khudaverdyan, Y. Miroshnychenko, A. Rauschenbeutel, and D. Meschede, “Neutral atom quantum register,” *Physical Review Letters*, vol. 93, no. 15, p. 150501, 2004.

[65] Y. S. Shao, B. Reagen, G.-Y. Wei, and D. Brooks, “Aladdin: A pre-rtl, power-performance accelerator simulator enabling large design space exploration of customized architectures,” in *2014 ACM/IEEE 41st International Symposium on Computer Architecture (ISCA)*, 2014, pp. 97–108.

[66] B. J. Shastri, A. N. Tait, T. Ferreira de Lima, W. H. Pernice, H. Bhaskaran, C. D. Wright, and P. R. Prucnal, “Photonics for artificial intelligence and neuromorphic computing,” *Nature Photonics*, vol. 15, no. 2, pp. 102–114, 2021.

[67] J. E. Smith, “Space-time computing with temporal neural networks,” *Synthesis Lectures on Computer Architecture*, vol. 12, no. 2, pp. i–215, 2017.

[68] ———, “Space-time algebra: A model for neocortical computation,” in *2018 ACM/IEEE 45th Annual International Symposium on Computer Architecture (ISCA)*. IEEE, 2018, pp. 289–300.

[69] ———, “A temporal neural network architecture for online learning,” *arXiv preprint arXiv:2011.13844*, 2020.

[70] ———, “A macrocolumn architecture implemented with temporal (spiking) neurons,” *arXiv preprint arXiv:2207.05081*, 2022.

[71] ———, “Neuromorphic online clustering and classification,” *arXiv preprint arXiv:2310.17797*, 2023.

[72] R. Stoltz, M. Schmelz, V. Zaksarenko, C. Foley, K. Tanabe, X. Xie, and R. Fagaly, “Superconducting sensors and methods in geophysical

applications.” *Superconductor Science and Technology*, vol. 34, no. 3, p. 033001, 2021.

[73] S. S. Tannu, P. Das, M. L. Lewis, R. Krick, D. M. Carmean, and M. K. Qureshi, “A case for superconducting accelerators,” in *Proceedings of the 16th ACM International Conference on Computing Frontiers*, ser. CF ’19. New York, NY, USA: Association for Computing Machinery, 2019, p. 67–75. [Online]. Available: <https://doi.org/10.1145/3310273.3321561>

[74] A. Thomas, “Memristor-based neural networks,” *Journal of Physics D: Applied Physics*, vol. 46, no. 9, p. 093001, 2013.

[75] G. Tzimpragos, D. Vasudevan, N. Tsiskaridze, G. Michelogiannakis, A. Madhavan, J. Volk, J. Shalf, and T. Sherwood, “A computational temporal logic for superconducting accelerators,” in *Proceedings of the Twenty-Fifth International Conference on Architectural Support for Programming Languages and Operating Systems*, ser. ASPLOS ’20. New York, NY, USA: Association for Computing Machinery, 2020, p. 435–448. [Online]. Available: <https://doi.org/10.1145/3373376.3378517>

[76] G. Van der Sande, D. Brunner, and M. C. Soriano, “Advances in photonic reservoir computing,” *Nanophotonics*, vol. 6, no. 3, pp. 561–576, 2017.

[77] P. Vellaisamy, H. Nair, V. Ratnakaram, D. Gupta, and J. Paul Shen, “Tnngen: Automated design of neuromorphic sensory processing units for time-series clustering,” *IEEE Transactions on Circuits and Systems II: Express Briefs*, vol. 71, no. 5, pp. 2519–2523, 2024.

[78] P. Vellaisamy, H. Nair, V. Ratnakaram, D. Gupta, and J. P. Shen, “Tnngen: Automated design of neuromorphic sensory processing units for time-series clustering,” *IEEE Transactions on Circuits and Systems II: Express Briefs*, 2024.

[79] J. Weng, S. Liu, V. Dadu, Z. Wang, P. Shah, and T. Nowatzki, “Dsagen: Synthesizing programmable spatial accelerators,” in *2020 ACM/IEEE 47th Annual International Symposium on Computer Architecture (ISCA)*, 2020, pp. 268–281.

[80] R. S. Williams, “How we found the missing memristor,” *IEEE spectrum*, vol. 45, no. 12, pp. 28–35, 2008.

[81] W. Won, T. Heo, S. Rashidi, S. Sridharan, S. Srinivasan, and T. Krishna, “Astra-sim2.0: Modeling hierarchical networks and disaggregated systems for large-model training at scale,” in *2023 IEEE International Symposium on Performance Analysis of Systems and Software (ISPASS)*, 2023, pp. 283–294.

[82] D. Wu, J. Li, R. Yin, H. Hsiao, Y. Kim, and J. S. Miguel, “uGEMM: Unary Computing Architecture for GEMM Applications,” in *International Symposium on Computer Architecture*, 2020.

[83] D. Wu and J. S. Miguel, “uSystolic: Byte-Crawling Unary Systolic Array,” in *International Symposium on High-Performance Computer Architecture*, 2022.

[84] Y. N. Wu, J. S. Emer, and V. Sze, “Accelergy: An architecture-level energy estimation methodology for accelerator designs,” in *2019 IEEE/ACM International Conference on Computer-Aided Design (ICCAD)*, 2019, pp. 1–8.

[85] C. Xu, P. Sharma, T. Wang, and L. W. Wills, “Fast, robust, and transferable prediction for hardware logic synthesis,” in *2023 56th IEEE/ACM International Symposium on Microarchitecture (MICRO)*, 2023, pp. 167–179.

[86] S. Xu, X. Chen, Y. Wang, Y. Han, X. Qian, and X. Li, “Pimsim: A flexible and detailed processing-in-memory simulator,” *IEEE Computer Architecture Letters*, vol. 18, no. 1, pp. 6–9, 2018.

[87] C. Yakopcic, T. M. Taha, G. Subramanyam, R. E. Pino, and S. Rogers, “A memristor device model,” *IEEE electron device letters*, vol. 32, no. 10, pp. 1436–1438, 2011.

[88] K. Yamazaki, V.-K. Vo-Ho, D. Bulsara, and N. Le, “Spiking neural networks and their applications: A review,” *Brain sciences*, vol. 12, no. 7, p. 863, 2022.

[89] P. Yao, H. Wu, B. Gao, J. Tang, Q. Zhang, W. Zhang, J. J. Yang, and H. Qian, “Fully hardware-implemented memristor convolutional neural network,” *Nature*, vol. 577, no. 7792, pp. 641–646, 2020.

[90] R. Yin, A. Moitra, A. Bhattacharjee, Y. Kim, and P. Panda, “Sata: Sparsity-aware training accelerator for spiking neural networks,” *IEEE Transactions on Computer-Aided Design of Integrated Circuits and Systems*, 2022.